Short Paper

Optimizing a Viscoelastic Finite Element Model to Represent the Dry, Natural, and Moist Human Finger Pressing on Glass

Saekwang Nam and Katherine J. Kuchenbecker

***Abstract*—When a fingerpad presses into a hard surface, the development of the contact area depends on the pressing force and speed. Importantly, it also varies with the finger's moisture, presumably because hydration changes the tissue's material properties. Therefore, we collected data from one finger repeatedly pressing a glass plate under three moisture conditions, and we constructed a finite element model that we optimized to simulate the same three scenarios. We controlled the moisture of the subject's finger to be dry, natural, or moist and recorded 15 pressing trials in each condition. The measurements include normal force over time plus finger-contact images that are processed to yield gross contact area. We defined the axially symmetric 3D model's lumped parameters to include an SLS-Kelvin model (spring in series with parallel spring and damper) for the bulk tissue, plus an elastic epidermal layer. Particle swarm optimization was used to find the parameter values that cause the simulation to best match the trials recorded in each moisture condition. The results show that the softness of the bulk tissue reduces as the finger becomes more hydrated. The epidermis of the moist finger model is softest, while the natural finger model has the highest viscosity.**

Index Terms—Fingerpad, gross contact area, finite element modeling, moisture

I. Introduction

Roboticists can gain intuition about secure grasping mechanisms by understanding human fingers. One of the crucial factors to ensuring fingerpad friction seems to be increasing the contact area at initial contact; unlike many other types of non-lubricated contact, skin friction does not obey Amonton's empirical rules, which claim that the maximum static friction force is directly proportional to normal force and independent of the apparent contact area [1]. Such an argument has led researchers to have more interest in finger contact area (Fig. 1). For instance, Dzidek et al. observed finger-contact evolution to explain how soft surfaces create the feeling of a secure grip [2]. Additionally, Wiertlewski et al. experimentally confirmed that higher real contact area between a finger and a surface contributes to increasing frictional force [3].

The finger's contact area is highly dependent on its material characteristics. Viscoelasticity enables the finger skin to conform to the surface during contact and prevents a rapid return to its initial shape after detachment. Viscosity specifically causes the reaction force of the skin to depend on the indenter's pressing speed [4], and it increases the finger's mechanical impedance at higher tapping frequencies [5]. Traditionally, a lumped-parameter model has been used to characterize mechanical behavior like this. A four-parameter model adeptly represents the mechanical response of skin and muscle in mammals [6], [7]. The simpler standard linear solid model with Kelvin presentation (SLS-Kelvin) can capture the initial dynamic response against an external force with only three parameters (two springs and one damper) [8].

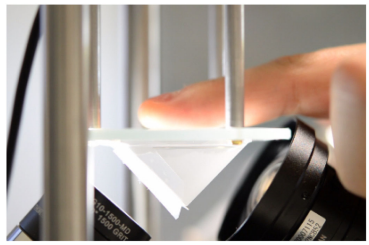

Fig. 1. A soft finger's contact area develops in various ways depending on its material properties and how it is pressed into the surface.

The finger consists of living tissues whose material properties vary depending on internal states. Interestingly, the material characteristics obtained from finger experiments with distinct conditions show a significant variation in values: Derler and Gerhardt reported that the elastic moduli of human skin in vivo vary over four to five orders of magnitude (4.4 kPa – 57 MPa) [1]. Sweat is thought to be a critical factor in altering these properties. When a finger is hydrated, the Young's modulus of its stratum corneum rises from that of glassy rubber to that of soft rubber [9], [10]. Therefore, the finger's material properties may largely depend on hydration.

This article investigates how a finger's material properties vary across diverse moisture conditions by determining the lumped parameters that best reproduce the finger's pressing behavior in each condition. As detailed in Section II and shown in the associated video, we record real finger deformations from one participant freely pressing on glass under three skin moisture conditions (dry, natural, and moist). The collected data are forces over time and finger-contact images that we post-process to obtain gross contact area. Such dynamic behaviors are simulated in a finite element finger model,

Manuscript received January 10, 2021; revised March 24, 2021; accepted April 28, 2021. Date of publication May 4, 2021; date of current version June 16, 2021. This article was recommended for publication by Associate Editor Dr. Seungmoon Choi and Editor-in-Chief Dr. Christian Duriez upon evaluation of the reviewers' comments. *(Corresponding author: Saekwang Nam.)*

The authors are with the Haptic Intelligence Department, Max Planck Institute for Intelligent Systems, 70569 Stuttgart, Germany (e-mail: s.nam@is.mpg.de; kjk@is.mpg.de).

This article has supplementary downloadable material available at https://doi.org/10.1109/TOH.2021.3077549, provided by the authors.

Digital Object Identifier 10.1109/TOH.2021.3077549

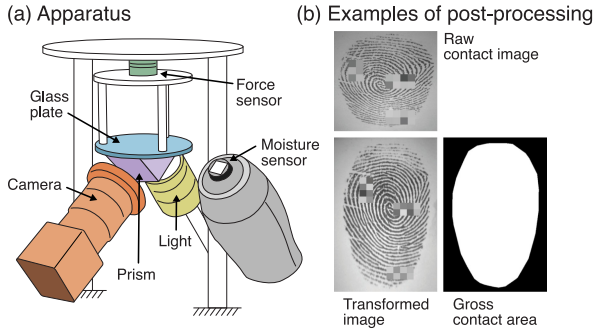

Fig. 2. (a) Our apparatus for capturing normal forces and contact images over time while a finger is pressing the glass plate [11]. The nearby moisture sensor measures the fingerpad's moisture level before and after contact. (b) The processing steps used to extract gross contact area from each raw contact image. Three regions of each fingerprint have been pixelized to prevent personal identification of the participant.

where we set the thin outer layer to deform linearly and made the bulk tissue behave based on the SLS-Kelvin model. Optimization enables us to find lumped parameter values that closely represent the behavior of the studied finger in each condition. As described in Section III, these analyses reveal that the bulk tissue gradually softens as the finger changes from dry to moist and that the outer skin layer (epidermis) becomes much softer for the moist finger alone. We also found that the bulk tissue's damping is highest for the natural finger, low for the dry finger, and almost zero for the moist finger. The article concludes in Section IV.

II. Methods

This section explains our data-collection procedures and how the data were post-processed for comparison with a finite element finger model. We then elucidate the finger model's design and the numerical simulation conditions. Lastly, we describe how we search for the optimal lumped parameters to represent the finger in each moisture condition.

A. Data Collection

We used the previously developed apparatus shown in Fig. 2(a) to record finger pressing force and contact area over time. During the finger contact, a strain-based force sensor (Nano17 Titanium SI-32-0.2 from ATI) measures the normal force at a high sampling rate (500 Hz) and resolution (1/171 N). An optical monochrome camera (DCC2340 M from Thorlabs) installed below the contact plate captures fingerprint images at 10 Hz. The light intensity contrast between the contact and non-contact fingerprint areas was emphasized by applying the prism-based frustrated total internal reflection (FTIR) principle [12]. The methods by which this apparatus achieves highly contrasted fingerprint images are explained in more detail by Nam *et al.* [11]. Lastly, a capacitive-type moisture sensor (Corneometer CM 825 from Courage + Khazaka electronic) is installed near the contact platform to measure the fingerpad moisture; it measures the moisture value of the outermost layer of the fingerpad in arbitrary units (a.u.) between 0 and 130.

Experiments were conducted with the left index finger of one human subject. Procedures were approved by the Max Planck Ethics Council (HI protocol 18-05B), and the subject provided informed consent. Before each trial, the subject was asked to immerse his fingerpad in isopropyl alcohol and let it evaporate to decrease skin moisture (dry finger), to do nothing to maintain a moderate moisture level (natural finger), or to perform repetitive physical exercises to sweat naturally (moist finger). The subject placed his fingerpad on the moisture sensor three times at the start of each trial. He then pressed his finger perpendicular to the center of the clean contact platform until the normal force reached 1.35 N, keeping the contact finger nearly parallel to the platform. Of particular note is that we did not restrict the pressing speed or time. Then, a visible cue on a computer screen indicated when to detach the finger. After lifting his finger off the glass plate, the subject pressed three more times on the moisture sensor. This procedure was repeated 45 times (blocks of 15 trials in the order of dry, natural, and moist finger).

B. Post-Processing

Each trial provides three types of data: the moisture measurements, an array of contact force vectors over time, and an array of finger contact images. The six moisture values from each trial were converted to one representative value by averaging. The small lateral forces were ignored, and each trial's normal force was down-sampled to match the frame rate of the camera. As summarized in Fig. 2(b), calculating an accurate gross contact area from a single raw contact image requires several processing steps that include geometric image corrections, the binarization of image pixels to identify contact pixels, and the extrapolation of gross contact area from the binary fingerprint image. The first step required camera calibration and the projective image transformation [13]. Next, the binarization was done by intensity thresholding [14], providing the real finger contact area. As the last step, the gross contact area was derived by extracting the convex hull of the pixels considered to be in contact and by multiplying the number of corresponding pixels with the pre-calculated area per pixel (0.000 986 mm^2/pixel).

C. Finite Element Model

To simulate the development of the contact area of the human finger pressing into a flat glass plate, we prepared a finite element (FE) finger model in COMSOL Multiphysics. Fig. 3(a) presents the axially symmetric 3D finger design. This model simulates finger behavior with a much lower computational load than a non-symmetric 3D model, allowing us to repeat the simulations with diverse parameter combinations. The dimensions of its components come from measurements of the subject's finger and the literature, as summarized in Table I. Note that the un-deformed finger was assumed to be an ellipsoid based on its length, width, and depth. The length and width were further turned into the semi-major radius of the ellipse model. The nail's dimensions were also obtained

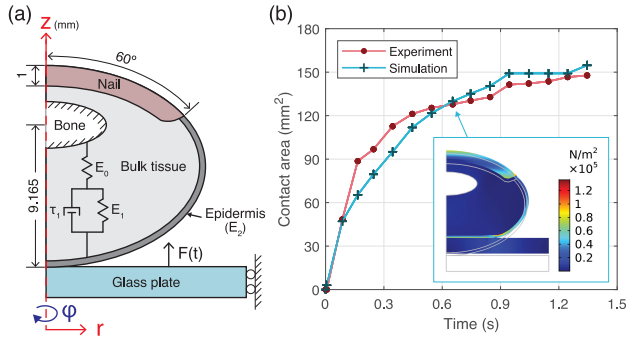

Fig. 3. (a) Our axially symmetric 3D finger model with lumped parameters and the conditions used for the simulations. (b) One recording of gross contact area over time for a natural finger pressing (the red line) compared with a simulation of the finger model pressing (the cyan line). Here, the model was simulated with the parameters of (E_0, E_1, τ_1, E_2) = (140 kPa, 20 kPa, 0.5 s, 2200 kPa); the inset image shows its deformation and von Mises stress at a time of 0.654 s.

from the subject's finger. The bone's size and location were estimated using relative proportions seen in the X-ray images of a finger [15].

In general, the finger's inner material is soft and suffused with fluid, while the thin outer layer is relatively hard. This knowledge led us to divide the finger into two layers (bulk tissue and epidermis). As the epidermis layer is dense and rubber-like [9], we assumed it as linearly elastic [16] and assigned it the parameter E_2. The bulk tissue's material properties were defined to follow the SLS-Kelvin model, in which a linear element (E_0) is connected to a Kelvin-Voigt model (E_1, τ_1) in series. We implemented this behavior within COMSOL using the SLS-Kelvin model [17]; we first specified the bulk tissue as a linear elastic material represented by E_0 and added an "external strain" component under the linear component. In one dimension, the external strain is defined via the following ordinary differential equation from the stress equilibrium equation:

$$\sigma = \sigma_{\eta_1} + \sigma_{G_1} = \eta_1 \frac{d\epsilon}{dt} + G_1 \epsilon \tag{1}$$

where η_1 and G_1 are respectively the viscosity and shear modulus, which allow us to calculate the model components $\tau_1 = \eta_1/G_1$ and $E_1 = 2G_1(1+\nu_1)$, where ν_1 is Poisson's ratio. Using the relaxation time τ_1 and $\sigma = \sigma_d/2$ (half of the deviatoric stress [18]), Eq. (1) can be further transformed to

$$2G_1\tau_1 \frac{d\epsilon}{dt} = \sigma_d - 2G_1\epsilon. \tag{2}$$

Equation (2) finally expands to the axially symmetric case with r, ϕ, and z axes such that

$$2G_1\tau_1 I_6 \begin{bmatrix} \partial\epsilon_r/\partial t \\ \partial\epsilon_\phi/\partial t \\ \partial\epsilon_z/\partial t \\ \partial\epsilon_{r\phi}/\partial t \\ \partial\epsilon_{rz}/\partial t \\ \partial\epsilon_{\phi z}/\partial t \end{bmatrix} = \begin{bmatrix} \sigma_d r - 2G_1\epsilon_r \\ \sigma_{d\phi} - 2G_1\epsilon_\phi \\ \sigma_{dz} - 2G_1\epsilon_z \\ \sigma_{dr\phi} - 2G_1\epsilon_{r\phi} \\ \sigma_{drz} - 2G_1\epsilon_{rz} \\ \sigma_{d\phi z} - 2G_1\epsilon_{\phi z} \end{bmatrix}. \tag{3}$$

TABLE I
CONSTANT PARAMETER VALUES FOR THE FE FINGER MODEL

Entity	Parameter	Value [unit]	Source
Finger	Semi-major radius	10.3 [mm]	-
	Semi-minor radius	6.5 [mm]	-
	Poisson's ratio	0.48 [-]	[19]
	Density	1000 [kg/m^3]	[20]
	Bulk modulus	10 [kPa]	[21]
Epidermis	Thickness	350 [μm]	[22]
Nail	Young's modulus	170 [MPa]	[23]
	Poisson's ratio	0.3 [-]	[23]
Bone	Semi-major radius	3.914 [mm]	[15]
	Semi-minor radius	1.495 [mm]	[15]
	Poisson's ratio	0.3 [-]	[23]
	Density	1960 [kg/m^3]	[24]
Glass plate	Young's modulus	90 [GPa]	[25]
	Poisson's ratio	0.2 [-]	[25]

Eq. (3) was entered as the "Domain ODE interface" under "Mathematics" physics in COMSOL. We assumed all deformations are isotropic and all materials are incompressible.

For simulations, we set the glass plate to press up into the finger and made the bone stationary. This reverse force application provides better structural stability than a finger pressing on a fixed glass plate [16]. The friction coefficient created between the fingerpad and the glass surface was set as 0.25 [26]. The actuation information (normal force over time) came from the force trajectory recorded in each of the 45 trials. Therefore, we could simulate the FE finger model with the same force and time conditions as each of the real trials collected in the experiment. At every time step, the software saved the finger's contact area (πr^2) by measuring the contact radius (r). For instance, Fig. 3(b) displays the simulated contact area compared with the measured gross contact area for a single trial.

D. Parameter Search

We seek the four lumped parameters (E_0, E_1, τ_1, and E_2) that cause the model's simulated contact area to evolve in the same way as the contact area measured in each experimental condition. Mathematically, the simulated area at time t_k and normal force F_k is $\hat{A}_k = f(E_0, E_1, \tau_1, E_2, t = t_k, F_N = F_k)$. After simulating the FE model with continuous time $\mathbf{t} \in \mathbb{R}^n$ and force $\mathbf{F} \in \mathbb{R}^n$ measured in the experiment, the area values would be $\hat{\mathbf{A}} \in \mathbb{R}^n$, where n is the number of measured data points for the selected finger pressing trial. We defined the cost function asthe mean squared error ($\text{MSE} = \frac{1}{n}\sum_{i=1}^{n}(\hat{A}_i - A_i)^2$) between the simulated and measured areas ($\hat{\mathbf{A}}$, $\mathbf{A}$) and looked for the parameter values producing the minimum cost. Our target is to identify the three different parameter sets that represent the three studied moisture conditions (dry, natural, moist). For each one, the objective is to find the parameter values that achieve the lowest sum of MSE values across the fifteen recorded trials ($J_C = \sum_{j=1}^{15} \text{MSE}_C^j$, simulating with force and time input data from the j-th pressing trial in moisture condition C).

We first investigated possible ranges for the parameters by repeatedly simulating the FE model with diverse combi-

nations. Possible values were chosen on the basis of known Young's moduli for the finger's layers (34 kPa for the fatty tissues and 80 kPa for the dermis [20]). We then manually tuned the parameters to identify extreme values for each parameter that caused the simulated area to generate a large MSE. Finally, we set the range of E_0 to be from 50 to 160 kPa, E_1 from 15 to 60 kPa, τ_1 from 0.01 to 0.80 s, and E_2 from 700 kPa to 2200 kPa. Furthermore, we confirmed the possibility of finding optimal parameter combinations within these ranges by computing J_C for each moisture condition at a brute-force grid of parameter combinations.

The search for the optimal parameter values was conducted with particle swarm optimization (PSO) [27]. This heuristic algorithm is highly suitable for our case because we do not know if our optimization problem is convex. We set the upper and lower bounds as the above-stated ranges and generated five candidate swarms to find the optimal values leading to the lowest cost. The swarms' initial positions were specified near the values generating the lowest cost from the brute-force search at each moisture condition. We ran the PSO algorithm three times in total, where the optimized parameters after each run represent the mechanical behavior of the finger in the dry, natural, or moist condition.

III. Results and Discussion

This section first presents the measurements from the human-subject experiment and describes how the post-processed data differ across moisture conditions. Next, it provides and discusses the sets of model parameters yielded by the optimization process for the three moisture conditions.

A. Measured Gross Contact Area by Force and Time

Fig. 4(a) shows the average moisture values recorded from the 45 pressing trials. The means and standard deviations are 37.56 $\pm$ 3.34, 69.31 $\pm$ 6.54, and 105.33 $\pm$ 4.93 for the dry, natural, and moist fingers, respectively. The broad overall range and lack of overlap between the three conditions indicates that the experimental methods effectively modified the participant's finger moisture, as desired.

The moisture level was also seen to affect the finger's gross contact area. When compared at the same force levels, the gross contact area was larger when the fingerpad was moist compared to dry or natural (Fig. 4(b)). In an ideal case where the finger is modeled as a purely elastic sphere (with no layers, bone, fingernail, or friction), its contact area on a flat plate can be calculated from normal force using a power law such as $A = k{F_N}^m$, where A and F_N are the gross contact area and the applied normal force, respectively [28], [29]. We fit this equation to the aggregate data from each condition to understand the general trends; the coefficient k increased as the finger's state moved from dry to moist, allowing the moist finger to produce a larger contact area at the same force. The fitted exponent values m were 0.67, 0.68, and 0.50 for the pressing trials of the dry, natural, and moist finger, respectively. They are each close to the theoretical value of 2/3 [30] or the value

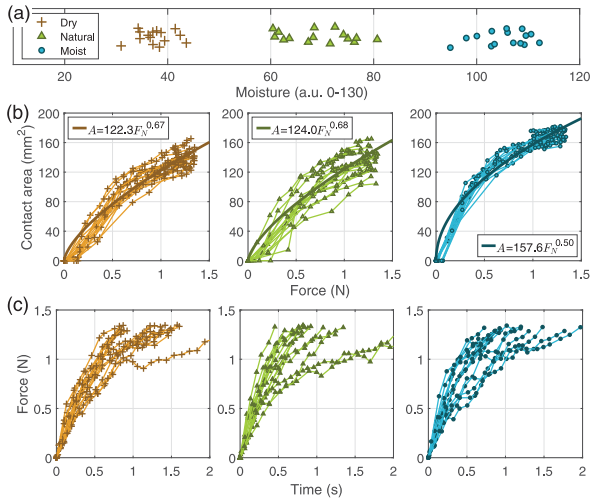

Fig. 4. Measured data after the post-processing. (a) The moisture values from the 45 trials are clearly distributed into three groups. (b) The way the gross contact area increases as a function of pressing force differs somewhat across moisture conditions; the fitted equation is based on the theoretical relationship between contact area and normal force for an elastic sphere. (c) Within each condition, the subject sometimes pressed quickly and sometimes much more slowly.

of 0.538 reported in a similar experiment on the index finger [31].

The power law formulation makes sense only if the finger is purely elastic. However, fingers have viscoelastic material properties, so the development of the contact area depends on the rate at which the finger is pressed into the surface. Fig. 4(c) shows that the participant pressed into the glass at widely varying speeds, taking between about 0.5 s and 2 s to reach the target normal force of 1.35 N across different trials in each condition. Visual inspection of Fig. 4(b) hints at lower contact area for the fast finger pressing trials (lines with fewer data points) in the dry and natural conditions, with little variation across the moist trials. For comparison with the optimized FE models, we also calculated the sums of MSE for the power-law fit to each moisture condition's contact area results: $J_{\mathrm{dry}} = 2650$ mm^4, $J_{\mathrm{natural}} = 4767$ mm^4, and $J_{\mathrm{moist}} = 1807$ mm^4.

Meanwhile, it is interesting to note that the theoretical exponent value ($m = 2/3$) is derived from the assumption that purely elastic spheres experience contact without adhesion. We believe that the critical difference in the fitted value for the moist finger ($m = 0.50$) from the other two values is due to a softer epidermis. At low normal force, a soft outer layer causes a larger contact area, decreasing m.

B. Optimized Parameter Values

After running the PSO algorithm, we extracted the top five parameter sets for simulating the finger's pressing behavior in each of the three studied moisture conditions, as shown in Fig. 5. The sums of MSE values are all at least 500 mm^4 lower than the corresponding best-fit power laws shown in Fig. 4(b), showing that our finite element model was able to represent the experimental results better than standard theory.

Dry finger					Natural finger					Moist finger				
E_0 (kPa)	E_1 (kPa)	τ_1 (s)	E_2 (kPa)	$\sum$MSE (mm^4)	E_0 (kPa)	E_1 (kPa)	τ_1 (s)	E_2 (kPa)	$\sum$MSE (mm^4)	E_0 (kPa)	E_1 (kPa)	τ_1 (s)	E_2 (kPa)	$\sum$MSE (mm^4)
95.2	44.3	0.07	1652	2135	155.0	22.0	0.44	1795	2886	160.0	15.0	0.01	700	1255
95.1	44.3	0.07	1652	2142	155.2	22.0	0.44	1800	2919	141.8	15.0	0.01	700	1271
95.0	44.3	0.07	1653	2150	156.7	22.0	0.45	1706	2933	104.7	15.0	0.01	700	1277
94.5	44.5	0.07	1660	2166	155.2	21.7	0.46	1739	2936	160.0	15.9	0.22	797	1350
93.4	46.2	0.04	1669	2293	155.8	22.6	0.44	1740	3050	64.0	15.4	0.03	1719	1352

Fig. 5. Top candidates for the lumped parameter values found by the particle swarm optimization algorithm, as well as the resulting MSE sums. The dashed lines indicate the boundaries where the sum of the MSE increases substantially compared to the fitting error of the top candidates.

Looking at the optimized parameter values, we found that the bulk tissue's composite steady-state elasticity ($E = 1/(1/E_0 + 1/E_1)$) decreases as the finger becomes hydrated (E = 30.23 kPa for dry, 19.27 kPa for natural, and 13.71 kPa for moist). These three values are consistent with those from an experiment by Maeno et al. who found the integrated Young's modulus considering both fatty tissue (34 kPa) and the dermis layer (80 kPa) is around 23.9 kPa [20]. We expect the finger softening may be caused by water filling in the eccrine sweat glands as the finger becomes moister. It is known that sweat gland density in the finger's volar region is the second-highest in the body (after the toe) [32]; the permeated liquid may allow deformations of the surrounding solid tissue mainly in the dermis layer.

The moist finger model had the lowest value (700 kPa) for the Young's modulus of the epidermis layer (E_2), whereas the corresponding moduli for the dry (1652 kPa) and natural (1795 kPa) fingers were similar. It is imaginable that the sweat excreted from the moist finger greatly softens that layer of skin. However, wiping the fingerpad with alcohol seems to reduce the epidermis layer's stiffness only slightly. Nonetheless, it may somewhat harden the bulk tissue, which is much softer than the epidermis. Considering that the sweat glands are located in the dermis, which is part of the bulk tissue in our model, we speculate that the alcohol may remove the sweat not only from the skin's surface but also from the sweat glands themselves. Alternatively, the alcohol may remove skin oils that naturally soften the interior tissue of the finger, or it may cool off the finger enough to change its internal material properties.

To better elucidate the optimal parameter sets chosen for the three conditions, we selected and plotted three experimental trials that had very similar force trajectories over time, as seen in Fig. 6. Although the subject pressed in almost the same way, the contact area trajectories differ, with the dry finger showing a slightly lower contact area than the natural finger, and the moist finger achieving a much higher contact area than the other two conditions. Although this plot might lead one to believe that the dry and natural finger have similar parameter values, our optimization results showed distinct optimal parameter sets. The bulk tissue of the dry finger is stiffer (higher composite stiffness from E_0 and E_1) and much less damped (lower τ_1)

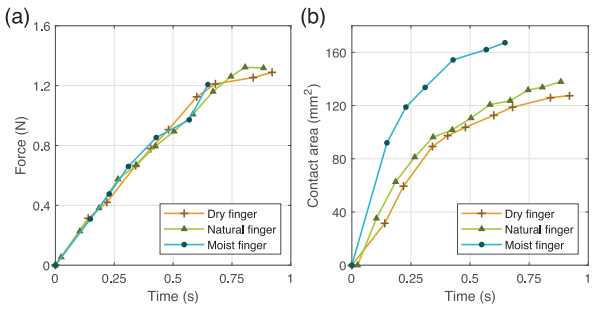

Fig. 6. One selected trial from each experimental condition. (a) The subject increased his pressing force in a very similar way for all three trials. (b) The resulting contact area over time differs across conditions.

than the natural finger. The same observation can be seen in Fig. 4; although the distributions of pressing force over time are similar for the dry and natural fingers (Fig. 4(c)), the distribution of the contact area is broader for the natural finger (Fig. 4(b)), implying a higher value of τ_1. In other words, the natural finger's behavior seems to depend more on pressing rate than the artificially dried finger's behavior does. In contrast, the moist finger's behavior is almost rate independent, with optimization yielding the minimum possible value for τ_1. Indeed, the contact area trajectories for the moist finger are closely clustered together in Fig. 4(b) despite the different pressing force trajectories applied by the subject. We speculate that the repeated exercise performed in the study caused a significant increase in the circulation of blood through the subject's body, such that his finger's tissue rebounded almost instantly after deformation in the moist condition.

C. Limitations

Although encouraging, this research has some limitations that should be acknowledged. There are non-negligible differences between our FE model and the real finger. First, our axially symmetric 3D finger model cannot precisely simulate the contact area development made by a real finger. This limitation comes from our assumption that the real finger's shape is an axially symmetric ellipsoid, which enabled us to use a more computationally efficient model. Second, the contact angle of the finger varied slightly across trials; our experimental apparatus cannot measure this source of variation, nor does

it record the downward movement of the finger itself. Third, the epidermis layer's thickness could be locally different from that of the real finger; we used an average value based on prior research [22].

Next, there are challenges in precisely calculating gross contact area from our experimental data. Basing the area on a convex hull, which consists of many straight lines connecting neighboring pixels considered to be in contact, can cause a relatively large error compared with the true area if only sparse areas of the skin are contacting. This limitation especially arises at the initial phase of finger pressing. For instance, Fig. 6(b) shows that the initial contact area of the natural finger is nearly zero even though the force sensor is registering a small force. We found that this issue happens when the measured force is less than 0.2 N. However, only a few data points were measured in this range, so they had little effect on the MSE sum used for optimization. For higher forces, the number of straight lines defining the gross contact area for the dry finger was almost identical to that for the natural finger, even though the measured areas were somewhat different. We therefore believe that our approach accurately estimates gross contact area even for dry fingers.

Including more measurement data might have enabled us to obtain better-optimized parameter values. Another option could be to conduct the same experiment with more human subjects. However, we encountered a severe time bottleneck running the PSO algorithm, as it conducts hundreds of COMSOL simulations to find the optimized parameter values for only one subject. Although we did our best to decrease the computing time, including running simulations in parallel, it took nearly three weeks of computation to obtain the values reported in this paper (2 minutes/trial $\times$ 15 trials/condition $\times$ 3 conditions $\times$ 5 swarms/round $\times$ 60 rounds $=$ 27 000 minutes $\approx$ 19 days). Nevertheless, examining data from other subjects would definitely increase the reliability of the trends observed in our optimized values.

IV. Conclusion

This paper used careful experimental measurements and a lumped-parameter FE model to investigate how the material properties of the human finger vary with moisture. After bringing the subject's finger into a dry, natural, or moist state, we recorded its moisture level, pressing normal forces over time, and contact images over time with a custom-made apparatus. The finger-contact images were further processed to calculate gross contact area over time. We then generated an axially symmetric 3D FE finger model with a rigid bone, a deformable fingernail, SLS-Kelvin lumped parameters for the viscoelastic bulk tissue, and a linearly elastic outer layer (epidermis). This model simulates contact area development when the finger is dynamically pressed into a glass plate with a specified force trajectory over time. Particle swarm optimization for each moisture condition identified the values of the four lumped parameters that best match the set of fifteen experimentally measured contact area trajectories for that moisture condition. The three sets of optimized values show that the finger's bulk tissue becomes softer as it becomes hydrated, that Young's modulus of the epidermis is the lowest in the moist condition, and that damping is highest in the natural condition. We believe that these research results can help elucidate why human fingers are so good at securely grasping flat objects in diverse conditions.

Acknowledgment

The authors would like to thank the International Max Planck Research School for Intelligent Systems (IMPRS-IS) for supporting Saekwang Nam. They would like to also thank Mayumi Mohan, Hyunkyu Park, Metin Sitti, Peer Fischer, and the anonymous reviewers.

References

[1] S. Derler and L.-C. Gerhardt, "Tribology of skin: Review and analysis of experimental results for the friction coefficient of human skin," *Tribology Lett.*, vol. 45, no. 1, pp. 1–27, 2012.
[2] B. Dzidek, S. Bochereau, S. A. Johnson, V. Hayward, and M. J. Adams, "Why pens have rubbery grips," *Proc. Nat. Acad. Sci.*, vol. 114, no. 41, pp. 10864–10869, 2017.
[3] M. Wiertlewski, R. Fenton Friesen, and J. E. Colgate, "Partial squeeze film levitation modulates fingertip friction," *Proc. Nat. Acad. Sci.*, vol. 113, no. 33, pp. 9210–9215, 2016.
[4] V. Cârlescu, D. N. Olaru, G. C. Prisăcaru Oprian, R. t. tirbu, and J. Machado, "Influence of the indentation speed on viscoelastic behavior of the human finger," in *Proc. Int. Conf. Innov., Eng. Entrepreneurship*, 2019, pp. 143–150.
[5] E. R. Serina, C. D. Mote, and D. Rempel, "Force response of the fingertip pulp to repeated compression - effects of loading rate, loading angle and anthropometry," *J. Biomech.*, vol. 30, no. 10, pp. 1035–1040, 1997.
[6] U. Dinnar, "A note on the theory of deformation in compressed skin tissues," *Math. Biosci.*, vol. 8, no. 1, pp. 71–82, 1970.
[7] K. Shimoga and A. Goldenberg, "Soft robotic fingertips: Part II: Modeling and impedance regulation," *Int. J. Robot. Res.*, vol. 15, no. 4, pp. 335–350, 1996.
[8] A. Dey and P. Basudhar, "Applicability of burger model in predicting the response of viscoelastic soil beds," in *Proc. GeoFlorida Adv. Anal., Model. Des.*, 2010, pp. 2611–2620.
[9] M. J. Adams, B. J. Briscoe, and S. A. Johnson, "Friction and lubrication of human skin," *Tribology Lett.*, vol. 26, no. 3, pp. 239–253, 2007.
[10] B. N. J. Persson, A. Kovalev, and S. N. Gorb, "Contact mechanics and friction on dry and wet human skin," *Tribol. Lett.*, vol. 50, no. 1, pp. 17–30, 2013.
[11] S. Nam, Y. Vardar, D. Gueorguiev, and K. J. Kuchenbecker, "Physical variables underlying tactile stickiness during fingerpad detachment," *Front. Neurosci.*, vol. 14, pp. 1–14, 2020, Art. no. 235.
[12] S. Bochereau, B. Dzidek, M. Adams, and V. Hayward, "Characterizing and imaging gross and real finger contacts under dynamic loading," *IEEE Trans. Haptics*, vol. 10, no. 4, pp. 456–465, Oct. 2017.
[13] Z. Zhang, "A flexible new technique for camera calibration," *IEEE Trans. Pattern Anal. Mach. Intell.*, vol. 22, pp. 1330–1334, Dec. 2000.
[14] E. R. Davies, *Computer and Machine Vision: Theory, Algorithms*, Practicalities. New York, NY, USA: Academic Press, 2012.
[15] E. Carver, *Fingers, Hand and Wrist*. 2016. Accessed: Dec. 10, 2020. [Online]. Available: https://radiologykey.com/fingers-hand-and-wrist/
[16] J. Z. Wu, K. Krajnak, D. E. Welcome, and R. G. Dong, "Three-dimensional finite element simulations of the dynamic response of a fingertip to vibration," *J. Biomech. Eng.*, vol. 130, no. 5, pp. 1–8, 2008, Art. no. 054501.
[17] COMSOL Inc, *Generalized Kelvin Viscoelastic Material*. 2019. Accessed: Dec. 12, 2020. [Online]. Available: https://www.comsol.com/model/generalized-kelvin-viscoelastic-material-29761
[18] S. P. C. Marques and G. J. Creus, *Computational Viscoelasticity*. Springer Science & Business Media, 2012.
[19] Y. C. Fung, *Biomechanics: Mechanical Properties of Living Tissues*. Springer Science & Business Media, 2013.
[20] T. Maeno, K. Kobayashi, and N. Yamazaki, "Relationship between structure of finger tissue and location of tactile receptors," *Trans. Jpn. Soc. Mech. Eng. C*, vol. 63, no. 607, pp. 881–888, 1997.

[21] M. Ayyildiz, M. Scaraggi, O. Sirin, C. Basdogan, and B. N. J. Persson, "Contact mechanics between the human finger and a touchscreen under electroadhesion," *Proc. Nat. Acad. Sci.*, vol. 115, no. 50, pp. 12668–12673, 2018.

[22] H. Fruhstorfer, U. Abel, C.-D. Garthe, and A. Knüttel, "Thickness of the stratum corneum of the volar fingertips," *Clin. Anat.*, vol. 13, no. 6, pp. 429–433, 2000.

[23] J. Z. Wu, R. G. Dong, S. Rakheja, and A. W. Schopper, "Simulation of mechanical responses of fingertip to dynamic loading," *Med. Eng. Phys.*, vol. 24, no. 4, pp. 253–264, 2002.

[24] J. W. A. Fletcher, S. Williams, M. R. Whitehouse, H. S. Gill, and E. Preatoni, "Juvenile bovine bone is an appropriate surrogate for normal and reduced density human bone in biomechanical testing: A validation study," *Sci. Rep.*, vol. 8, no. 1, pp. 1–9, 2018.

[25] M. M. Gauthier, *Engineered Materials Handbook*. ASM International, 1995, vol. 1.

[26] S. M. Pasumarty, S. A. Johnson, S. A. Watson, and M. J. Adams, "Friction of the human finger pad: Influence of moisture, occlusion and velocity," *Tribology Lett.*, vol. 44, no. 2, p. 117, 2011.

[27] J. Kennedy and R. Eberhart, "Particle swarm optimization," in *Proc. IEEE Int. Conf. Neural Netw.*, vol. 4, 1995, pp. 1942–1948.

[28] B. Delhaye, P. Lefèvre, and J.-L. Thonnard, "Dynamics of fingertip contact during the onset of tangential slip," *J. Royal Soc. Interface*, vol. 11, no. 100, 2014, Art. no. 20140698.

[29] K. L. Johnson, *Contact Mechanics*. Cambridge, U.K.: Cambridge Univ. Press, 1987.

[30] B. M. Dzidek, M. J. Adams, J. W. Andrews, Z. Zhang, and S. A. Johnson, "Contact mechanics of the human finger pad under compressive loads," *J. Royal Soc. Interface*, vol. 14, no. 127, 2017, Art. no. 20160935.

[31] P. H. Warman and A. R. Ennos, "Fingerprints are unlikely to increase the friction of primate fingerpads," *J. Exp. Biol.*, vol. 212, no. 13, pp. 2016–2022, 2009.

[32] N. A. Taylor and C. A. Machado-Moreira, "Regional variations in transepidermal water loss, eccrine sweat gland density, sweat secretion rates and electrolyte composition in resting and exercising humans," *Extreme Physiol. Med.*, vol. 2, no. 1, pp. 1–29, 2013, Art. no. 4.